JOURNAL OF THERMOPHYSICS AND HEAT TRANSFER
Vol. 24, No. 3, July–September 2010

Advanced Radiation Calculations of Hypersonic Reentry Flows Using Efficient Databasing Schemes

I. Sohn,* A. Bansal,* and D. A. Levin†
Pennsylvania State University, University Park, Pennsylvania 16802
and
M. F. Modest‡
University of California, Merced, California 95343

DOI: 10.2514/1.45085

Efficient schemes for databasing emission and absorption coefficients are developed to model radiation from hypersonic nonequilibrium flows. For bound–bound transitions, spectral information including the line-center wavelength and emission and absorption coefficients is stored for typical air plasma species. Since the flow is nonequilibrium, a rate equation approach including both collisional and radiatively induced transitions is used to calculate the electronic state populations, assuming quasi steady state. The general Voigt line-shape function is assumed for modeling the line-broadening. The accuracy and efficiency of the databasing scheme was examined by comparing results of the databasing scheme with those of NEQAIR for the Stardust flowfield. An accuracy of approximately 1% was achieved with an efficiency about three times faster than the NEQAIR code.

Nomenclature

A	=	Einstein coefficient for spontaneous emission, s^{-1}
$A(c,i)$	=	Einstein coefficient for spontaneous emission from continuum state to state i, $cm^3\ s^{-1}$
$A(i,c)$	=	Einstein coefficient for photoionization from state i to continuum state, s^{-1}
$A(i,j)$	=	Einstein coefficient for spontaneous emission from state i to state j, s^{-1}
a_0	=	Bohr radius, 5.29167×10^{-9} cm
B	=	Einstein coefficient for stimulated emission and absorption, $(cm^3\text{-}\mu m)/(J\text{-}s)$
B_{V_U}	=	rotational constant, cm^{-1}
b	=	exponent
$\bar{C}, \bar{D}$	=	vector assembled by excitation rate coefficients of atom
$\bar{C}_m, \bar{D}_m$	=	vector assembled by excitation and dissociation rate coefficients of molecule
c	=	speed of light, 2.9979×10^{10} cm s^{-1}
D_w	=	Doppler line half-width, cm
d	=	parameter in the Voigt width [Eq. (34)]
d_{ff}	=	correction factor for free–free radiation
E_i	=	electronic term energy for atomic level i, cm^{-1}
E_k	=	kinetic energy of free electron, cm^{-1}
E_{emis}	=	total emission energy, W/cm^3
E_∞	=	ionization energy of an atom, cm^{-1}
e	=	electron charge, 4.8030×10^{-10} statC
F	=	rotational term energy for a molecule, cm^{-1}
F_i	=	assembled collisional and radiative coefficient of electronic state i
G	=	vibrational term energy for a molecule, cm^{-1}
GF	=	Gaunt factor for bound–free radiation
G_i	=	assembled collisional and radiative coefficient of electronic state i
g	=	degeneracy
H	=	data points of electron number density and electron temperature
h	=	Planck's constant, 6.6262×10^{-34} Js
J	=	rotational quantum number
j	=	data point index
$K(c,i)$	=	recombination rate coefficient of collisional transition from continuum state to state i, $cm^6\ s^{-1}$
$K(i,c)$	=	excitation rate coefficient of collisional transition from state i to continuum state, $cm^3\ s^{-1}$
K_{Wi}	=	heavy-particle-induced recombination rate coefficient, $cm^3\ s^{-1}$
$K^W(i,j)$	=	heavy-particle-induced molecular excitation rate coefficient from state i to state j, $cm^3\ s^{-1}$
$K^e(i,j)$	=	excitation rate coefficient of collisional transition from state i to state j by electron impact, $cm^3\ s^{-1}$
K^e_{ci}	=	electron-induced recombination rate coefficient, $cm^3\ s^{-1}$
k	=	Boltzmann's constant, 1.3806×10^{-23} JK^{-1}
l	=	number of electronic states for bound–free transition
l_m	=	number of electronic state energy levels for diatomic quasi steady state
M	=	matrix assembled excitation rate coefficients of atom
M_m	=	matrix assembled excitation and dissociation rate coefficients of molecule
m	=	mass, kg
max	=	maximum value of vibrational or rotational line
N	=	number density, cm^{-3}
n	=	principal quantum number
P	=	number of data points
Q	=	partition function
q	=	Franck–Condon factor
q_R	=	radiative heat flux, W/cm^2
R	=	transition moment, statC-cm
Re	=	electronic transition moment for a vibrational band (V_U, V_L) normalized by ea_0

Presented as Paper 2008-4019 at the 40th Thermophysics Conference, Seattle, WA, 23–26 June 2008; received 22 April 2009; revision received 2 March 2010; accepted for publication 2 March 2010.

*Graduate Student, Department of Aerospace Engineering. Student Member AIAA.

†Professor Department of Aerospace Engineering. Associate Fellow AIAA.

‡Shaffer and George Professor of Engineering, Department of Mechanical Engineering. Associate Fellow AIAA.

r = internuclear distance, units of length, not explicitly evaluated
S = rotational line-strength factor
T_e = electron temperature, K
T_{eL} = lower state electronic energy of the term symbol for molecular radiation, cm^{-1}
T_{eU} = upper state electronic energy of the term symbol for molecular radiation, cm^{-1}
T_{rot} = rotational temperature, K
T_{trn} = translational temperature, K
T_{vib} = vibrational temperature, K
V = vibrational quantum number
w_g = Gaussian width, Å
w_l = Lorentzian width, Å
w_s = Stark width, Å
$w_{s,0}$ = reference Stark width, Å
w_v = Voigt width, Å
X = horizontal coordinate of direct simulation Monte Carlo computational domain for the Stardust geometry, m
$X_{i,\text{data}}$ = emission or absorption coefficients from the database at the ith wavelength data point
$X_{i,\text{NEQ}}$ = emission or absorption coefficients from NEQAIR at the ith wavelength data point
Y = vertical coordinate of DSMC computational domain for the Stardust geometry, m
ΔE = net kinetic energy of a free electron, cm^{-1}
ΔH = data point interval
$\Delta\lambda$ = distance from line center, Å
ε = emission coefficient, $\text{W/cm}^3\text{-}\mu\text{m-sr}$
ε_λ^c = assembled parameter for emission coefficient, W/sr
κ = absorption coefficient, cm^{-1}
κ_λ^c = assembled parameter for absorption coefficient, cm^3
λ = wavelength, Å
$\tilde{\nu}$ = wave number, cm^{-1}
ρ = ratio of nonequilibrium electronic state population to equilibrium state
$\sigma_{\lambda H}$ = ionization cross section of hydrogen atom, cm^2
$\sigma_\lambda^{\text{bf}}$ = bound–free absorption cross section, cm^2
σ_H^{ff} = hydrogenic free–free cross section, cm^5
ϕ_λ = line-broadening function, μm^{-1}
χ = ratio of summation of nonequilibrium electronic state populations to that of equilibrium state
Ψ = vibrational wave function, units of length$^{-1/2}$, not explicitly evaluated

Subscripts

a = atom
c = center
E = equilibrium state
e = electron
emis = emission
end = ending data
H = hydrogenic
i, j = index of electronic state
init = initial data
k = kinetic
L = lower state
LU = lower to upper state
m = molecule
min = cutoff limit
NEQ = NEQAIR
n = principal quantum number
R = rotational state
U = upper state
UL = upper to lower state
V = vibrational state
W = heavy particle
λ = wavelength
$+$ = ion
∞ = ionization

Superscripts

bf = bound–free
c = constant
e = electronic state
ff = free–free
$*$ = normalized quantity

I. Introduction

HYPERSONIC vehicles reentering into Earth's atmosphere generate nonequilibrium flows consisting of dissociated and weakly ionized air species. These typical conditions exist behind a high Mach number shock wave leading to high temperatures that affect operational flight issues related to thermal protection system materials and radar communications. In addition, due to the high Mach number, radiation has an important role in generating heat loads to the vehicle surface, with contributions sometimes as high as 18% of the convective heat [1]. Modeling the radiative sources in hypersonic shock layers and fluxes to a spacecraft is a complex task and we mention here only some of the important work in this field. The Langley LORAN code [2] and the NEQAIR code [3] have been used extensively in many atmospheric entry radiative simulations. NEQAIR includes atomic bound–bound, bound–free, free–free transition, and line-by-line models for molecular bands. The LORAN model is similar to NEQAIR, and was developed to lower the computational cost of NEQAIR by using a smeared rotational band model for the molecular species. Both NEQAIR and LORAN use the quasi-steady-state (QSS) assumption to determine the electronic state population. More recently, Johnston [4] developed a radiation model that applied up-to-date atomic and molecular data for both the non-Boltzmann modeling of the radiating state and spectral distributions. In his model, an approximate atomic collisional radiative model was developed to calculate the electronic state populations of atomic species. For molecular radiation a simplified non-Boltzmann model for the molecular electronic state populations was developed by assuming that the contribution of electron-impact dissociation and heavy-particle-induced excitation processes may be neglected. The smeared rotational band model was chosen to reduce the computational cost for molecular radiation. In nonequilibrium flows, the radiation field may also affect the population of electronic states to the extent that a coupled radiative transport solution is required for an exact solution. Therefore, it becomes imperative to determine emission and absorption coefficients in an efficient manner such that a large number of solutions of the radiative transport equation (RTE) may be performed.

In this work, we develop an efficient databasing scheme for generating spectral coefficients using the NEQAIR code. In contrast to the models mentioned above, we use assembled parameters, extracted directly from NEQAIR, to calculate spectral line strengths. One of the main challenges in developing the databasing scheme was to incorporate the QSS procedure, which includes the calculation of about 40 electronically excited states for atomic oxygen and nitrogen. Also, because the reentry flows are optically thick to maintain accuracy in computing the radiative heat loads, the databasing procedure has to incorporate the Voigt line shape. The accuracy and efficiency of atomic and diatomic emission and absorption coefficients obtained from the new database are examined for a flow condition close to peak heating along the Stardust reentry trajectory. Since atomic radiation is dominant for the hypersonic reentry flow conditions under consideration here, only the accuracy of the atomic spectral coefficients generated from the database are investigated in this paper. In the final section, the accuracy of the databasing scheme are examined by comparing the radiative heat fluxes using the database with those obtained directly from NEQAIR. The efficiency of the databasing scheme is quantified and the radiative heat generation using the new database are calculated for a Stardust reentry flowfield.

II. Databasing Schemes for Atomic Species

In this section, the basic spectral relationships for the emission and absorption coefficients are introduced. The databasing strategy is examined and the variables that are databased are defined in terms of the spectral quantities.

A. Basic Relations of Radiation by Atomic Species

There are three radiative mechanisms in a radiating nonscattering medium: spontaneous emission, stimulated emission and absorption. The spontaneous spectral emission coefficient is defined as [3]

$$\varepsilon_\lambda = g_U N_U A_{\mathrm{UL}} hc\phi_\lambda \frac{1}{\lambda}\frac{1}{4\pi} \tag{1}$$

Stimulated emission and absorption, unlike spontaneous emission, are caused by the presence of photons in the vicinity of the emitting or absorbing species. The effective volumetric absorption coefficient is obtained in terms of the stimulated emission and absorption coefficients, as given by [3]

$$\kappa_\lambda = (g_L N_L B_{\mathrm{LU}} - g_U N_U B_{\mathrm{UL}})\frac{h}{\lambda}\phi_\lambda \tag{2}$$

Using detailed balance [3,5], $g_L B_{\mathrm{LU}} = g_U B_{\mathrm{UL}}$, the absorption coefficient expression can be reduced to

$$\kappa_\lambda = (N_L - N_U) g_U B_{\mathrm{UL}} \frac{h}{\lambda}\phi_\lambda \tag{3}$$

Normalized emission and absorption coefficients can be defined by dividing Eqs. (1) and (3) by the number density of the radiating species, N_a, giving

$$\varepsilon^*_\lambda = \frac{\varepsilon_\lambda}{N_a} = \varepsilon^c_\lambda \left(\frac{N_U}{N_a}\right)\phi_\lambda \tag{4}$$

$$\kappa^*_\lambda = \frac{\kappa_\lambda}{N_a} = \kappa^c_\lambda \left(\frac{N_L}{N_a} - \frac{N_U}{N_a}\right)\phi_\lambda \tag{5}$$

where ε^c_λ and κ^c_λ are defined as

$$\varepsilon^c_\lambda = g_U A_{\mathrm{UL}} h \frac{c}{\lambda}\frac{1}{4\pi} \tag{6}$$

$$\kappa^c_\lambda = g_U B_{\mathrm{UL}} \frac{h}{\lambda} \tag{7}$$

and

$$B_{\mathrm{UL}} = \frac{\lambda^5}{8\pi hc} A_{\mathrm{UL}} \tag{8}$$

for all bound–bound transitions at the specific line-center wavelength [3,5,6]. This leads to an important result for organizing the database; i.e., ε^c_λ and κ^c_λ are independent of parameters, such as ion and electron number densities and temperatures.

There are two other transition mechanisms that lead to a change of energy level by emission or absorption of a photon. Transitions from a bound to a dissociated state, known as bound–free transitions and the reverse transitions, called free-bound transitions are two such mechanisms. Also transitions between two continuum states, called free–free transitions, are possible mechanisms caused by photon-atom interactions. For atomic radiation, the bound–bound transitions are the largest contributions to the radiation compared with bound–free and free–free transitions. The bound–free radiation occurs when the upper state is in the ionized, or continuum state. In that case, the wavelength of the transition is determined by the kinetic energy of the free electron, E_k, or

$$\lambda = \frac{1}{\Delta E} = \frac{1}{E_\infty - E_i + E_k} \tag{9}$$

where E_∞ is the ionization potential of the atom and E_i is the energy of the ith bound level. Since the electron kinetic energy E_k is continuously distributed according to a Maxwellian distribution, radiation from bound–free transitions is spectrally continuous. The bound–free absorption cross section $\sigma^{\mathrm{bf}}_\lambda$ is defined in terms of the ionization cross section of the hydrogen atom $\sigma_{\lambda H}$ multiplied by a correction factor known as the Gaunt factor [7]. The hydrogenic cross sections are defined by Kramer's formula [8] as

$$\sigma_{\lambda H} = 7.9 \times 10^{-18} n \left(\frac{\lambda}{\lambda_n}\right)^3 \tag{10}$$

where the value of λ_n is given as $\lambda_n = n^2 10^8 / I_H$, I_H is the ionization potential of atomic hydrogen, 109, 679 cm^{-1}, and n is the principal quantum number. The Gaunt factor GF_λ is defined as

$$\mathrm{GF}_{\lambda,i} = \frac{\sigma^{\mathrm{bf}}_{\lambda,i}}{\sigma_{\lambda H}} \tag{11}$$

The Gaunt factor is determined by comparing the cross sections with those of Peach [7]. Note that for a specific electronic state $\sigma^{\mathrm{bf}}_\lambda$ is only a function of wavelength. Finally, the bound–free absorption coefficient for each energy level is obtained by the bound–free cross section multiplied by the electronic state population as

$$\kappa^{\mathrm{bf}}_\lambda = \sum_{i=1}^{l} (\sigma^{\mathrm{bf}}_{\lambda,i} N_i) \tag{12}$$

where l stands for the number of electronic states modeled in the NEQAIR database. For atomic O and N, there are $l = 15$ out of the total 19 states and 14 out of 22, respectively. The remaining levels do not contribute to the sum because they are assumed to be quasi-nonbound or existing in the continuum. The bound–free emission is calculated from Eq. (12) using relations given by [3]

$$\varepsilon^{\mathrm{bf}}_\lambda = \sum_{i=1}^{l} \left(\sigma^{\mathrm{bf}}_{\lambda,i} N_i \frac{2hc^2}{\lambda^5 (N_i/N_U - 1)}\right) \tag{13}$$

where N_U is chosen as the population at the ionization limit given by

$$N_U = 2.07 \times 10^{-16} \frac{N_+ N_e}{Q^e_+ T_e^{1.5}} \exp\left(-\frac{hc}{k}\frac{E_\infty}{T_e}\right) \tag{14}$$

The value of 2.07×10^{-16} is calculated from the expression of $(h^2/(2\pi m_e k))^{3/2}/2$ given by [3]. Free-free transition occurs when an electron in the vicinity of an ion or an atom is decelerated and emits radiation to conserve energy. The free–free absorption coefficient divided by the atomic number density, employing the hydrogenic free–free cross section, $\sigma^{\mathrm{ff}}_{\lambda H}$, is calculated as [3]

$$\frac{\kappa^{\mathrm{ff}}_\lambda}{N_a} = \frac{N_+ N_e}{N_a} \sigma^{\mathrm{ff}}_{\lambda H} (1 + d_{\mathrm{ff}}) \tag{15}$$

where d_{ff} is a correction factor for the free–free cross section of nonhydrogenic atomic species [7]. The free–free emission is calculated using the blackbody function given by [3]

$$\varepsilon^{\mathrm{ff}}_\lambda = \kappa^{\mathrm{ff}}_\lambda \frac{2hc^2}{\lambda^5 [\exp(hc/\lambda k T_e) - 1]} \tag{16}$$

B. Calculation of Excited State Populations: Quasi-Steady-State Assumption

Under nonequilibrium flow conditions, the atomic electronic states are excited and deexcited by collisional and radiative processes. When an atom collides with other atoms, molecules, or electrons, the electronic states potentially become excited. Collision induced electronic transitions in an atomic or molecular system are particularly effective when the collider is an electron. Specifically, when a free electron with large energy collides with an atom in a bound state, the energy of the free electron can be transferred to the atom in the form of electronic state excitation. In this case, the excitation rate from the initial state i to the final state j is $K^e(i, j) N_i N_e$. In

nonequilibrium flow conditions, radiative transitions also have an important role in determining the electronic state of neutral species. A summary of the excitation/deexcitation processes of atoms may be written as

$$\mathrm{O}(i) + \mathrm{e}^- \overset{K^e(i,j)}{\longleftrightarrow} \mathrm{O}(j) + \mathrm{e}^- \tag{17}$$

$$\mathrm{O}(i) + \mathrm{e}^- \overset{K(i,c)}{\longleftrightarrow} \mathrm{O}^+ + 2\mathrm{e}^- \tag{18}$$

$$\mathrm{O}(i) \overset{A(i,j)}{\longleftrightarrow} \mathrm{O}(j) + h\nu \tag{19}$$

$$\mathrm{O}(i) + h\nu \overset{A(i,c)}{\longleftrightarrow} \mathrm{O}^+ + \mathrm{e}^- \tag{20}$$

where $\mathrm{O}(i)$ and O^+ represent an atomic species of electronic energy level i and its ion, respectively. Under nonequilibrium flow conditions, there are not enough collisions to describe the electronic states by a Boltzmann distribution; therefore, a rate equation approach must be needed to calculate the electronic state populations [5]. The time rate of change of number density N_i is given by the difference between the sum of the rates of all collisional and radiative transitions that populate and depopulate state i:

$$\frac{\partial N_i}{\partial t} = \text{formation–removal} \tag{21}$$

where the population and the depopulation of the ith state may be expressed for formation as

$$\sum_{j=1}^{l} K^e(j,i)N_jN_e + K(c,i)N_+N_e^2 + \sum_{j=1}^{l} A(j,i)N_j + A(c,i)N_+N_e \tag{22}$$

and for removal as

$$\sum_{j=1}^{l} K^e(i,j)N_iN_e + K(i,c)N_iN_e + \sum_{j=1}^{l} A(i,j)N_i + A(i,c)N_i \tag{23}$$

When the rate of change of N_i on the left-hand side is much smaller than both the sum of all population rates and all depopulation rates on the right-hand side, the QSS condition holds. For this condition, the left-hand side is set to zero and the system of differential equations can be rewritten as a set of algebraic equations as follows:

$$\left[\sum_{j=1}^{l} K^e(i,j) + K(i,c) + \frac{\sum_{j=1}^{l} A(i,j) + A(i,c)}{N_e}\right]\rho_i - \sum_{j=1}^{l}\left[K^e(i,j) + \frac{N_{jE}}{N_{iE}}\frac{A(j,i)}{N_e}\right]\rho_j = K(i,c) + A(c,i)\frac{N_+}{N_{iE}} \tag{24}$$

where

$$K^e(i,j)N_{iE} = K^e(j,i)N_{jE} \qquad K(i,c)N_{iE} = K(c,i)N_+N_e \tag{25}$$

$$\rho_i = N_i/N_{iE} \tag{26}$$

and N_{iE} is the number density of the ith state in equilibrium. The symbols N_+, N_e, N_a, and T_e are the ion, electron, atom number densities, and electron temperature, respectively. Since the sum over all N_i must be equal to the total number density of the atomic species, or

$$\sum_{i=1}^{l} \frac{N_{iE}}{N_e}\rho_i = \chi\frac{N_{aE}}{N_e} \tag{27}$$

Eqs. (24) and (27) can be rewritten in the matrix form of

$$M\bar{\rho} = \bar{C} + \bar{D}\frac{N_a}{N_{aE}} \tag{28}$$

where $\chi = N_a/N_{aE}$ and

$$N_{aE} = \sum_{i=1}^{l} N_{iE}$$

and the matrix M and vectors $\bar{C}$ and $\bar{D}$ are functions of only T_e and N_e [5]. Finally, the normalized population can be expressed as

$$\frac{N_i}{N_a} = F_i(T_e,N_e)\frac{N_+}{N_a} + G_i(T_e,N_e) \tag{29}$$

where

$$F_i(T_e,N_e) = M^{-1}\bar{C}\frac{N_{iE}}{N_+} \qquad G_i(T_e,N_e) = M^{-1}\bar{D}\frac{N_{iE}}{N_{aE}} \tag{30}$$

The two functions F_i and G_i contain the effects of both collisional and radiative transitions for the excitation of atoms in the ith electronic energy state.

C. Strategy for Generating Databases of Atomic Spectral Quantities

For the bound–bound transitions, the line-strength factors ε_λ^c and κ_λ^c for the emission and absorption coefficients given by Eqs. (6) and (7), respectively, are obtained from NEQAIR [3]. The line-center wavelengths at which the bound–bound transitions occur and the potential upper and lower electronic states for each bound–bound transition are also obtained from NEQAIR. Tables 1 and 2 show the first five line-strength factors ε_λ^c and κ_λ^c, the line-center wavelength, and the upper and lower electronic energy levels for each bound–bound transition for atomic O and N, respectively. The normalized electronic state populations calculated using the QSS assumption are given by Eq. (29). In this equation, since the ion and atomic number densities will be obtained from the flowfield solution directly, one needs to database values of $F_i(T_e,N_e)$ and $G_i(T_e,N_e)$ at various values of T_e and N_e to calculate the normalized electronic state populations for each electronic state i. Cubic spline interpolation of F_i and G_i at arbitrary T_e and N_e values may then be used. The data set for $F_i(T_e,N_e)$ and $G_i(T_e,N_e)$ are defined at 50 N_e values and 70 T_e values, with N_e varying from 10^{13} to 4×10^{16} cm^{-3} and T_e ranging from 1000 to 28,000 K, with a equally spacing given by

$$H_j = (H_{\text{init}}^{0.1} + (j-1)\Delta H^{0.1})^{10} \tag{31}$$

where $\Delta H^{0.1} = (H_{\text{end}}^{0.1} - H_{\text{init}}^{0.1})/(P-1)$. Here, P is the number of data points, 50 for N_e and 70 for T_e, and j denotes the data point

Table 1 Data sets for ε_λ^c and κ_λ^c of atomic O

			Electronic levels	
Wavelength, Å	ε_λ^c, W/sr	κ_λ^c, cm^3	Upper	Lower
807.365	1.374×10^{-10}	3.957×10^{-24}	19	1
879.450	7.007×10^{-11}	3.095×10^{-24}	19	1
879.538	2.156×10^{-10}	9.526×10^{-24}	19	1
880.599	5.742×10^{-11}	2.553×10^{-24}	19	1
880.648	4.252×10^{-11}	1.891×10^{-24}	19	1

Table 2 Data sets for ε_λ^c and κ_λ^c of atomic N

			Electronic levels	
Wavelength, Å	ε_λ^c, W/sr	κ_λ^c, cm^3	Upper	Lower
1101.276	2.841×10^{-11}	3.8633×10^{-24}	12	2
1134.725	6.962×10^{-11}	1.0966×10^{-23}	5	1
1134.975	1.392×10^{-10}	2.2012×10^{-23}	5	1
1135.535	1.837×10^{-10}	2.9113×10^{-23}	5	1
1164.412	2.605×10^{-13}	4.6820×10^{-25}	10	2

index, $1 \le j \le P$. The form of Eq. (31) reduces the computation time for interpolation of F_i and G_i at any N_e and T_e conditions because searching for a desired point is faster using equally spaced rather than non-equally-spaced data points. The total size of the database of $F_i(T_e, N_e)$ and $G_i(T_e, N_e)$ of each atomic species O and N is about 6.2 MB. This approach allows us to incorporate all of the models developed over many years in NEQAIR for the QSS model as well as permit the efficient recalculation of the database as the QSS model evolves.

To complete the database formulation, we need to specify the line shape. The Voigt line-shape function is selected because it is the most general form of line-broadening. It considers both thermal and collisional broadening effects, as required to properly simulate line-broadening under nonequilibrium flow conditions. The approximate formula of Whiting [9] is given as

$$\begin{aligned}\phi_\lambda = {} & [(1 - w_l/w_v)\exp(-2.772(\Delta\lambda/w_v)^2) \\ & + (w_l/w_v)/\{1 + 4(\Delta\lambda/w_v)^2\} + 0.016(w_l/w_v) \\ & \times (1 - w_l/w_v)(\exp\{-0.4(\Delta\lambda/w_v)^{0.25}\} \\ & - 10/\{10 + (\Delta\lambda/w_v)^{2.25}\})]/[w_v\{1.065 \\ & + 0.447(w_l/w_v) + 0.058(w_l/w_v)^2\}] \end{aligned} \tag{32}$$

where w_l and w_v denote the Lorentzian and Voigt widths, respectively, and $\Delta\lambda$ is given by

$$\Delta\lambda = \lambda - \lambda_c \tag{33}$$

The Voigt width is calculated from the following approximation [10]:

$$\begin{aligned} w_v = {} & [1 - 0.18121 \times (1 - d^2) - (0.023665\exp(0.6d) \\ & + 0.00418\exp(-1.9d) \times \sin(\pi d)](w_l + w_g) \end{aligned} \tag{34}$$

where $d = (w_l - w_g)/(w_l + w_g)$ and w_g is Gaussian or Doppler width. The main contribution to the Lorentzian width for hypersonic flow conditions is due to Stark broadening caused by high energy electron collisions with atoms. The Stark line-broadening widths, w_s, at half-line-center peak height are calculated for each individual line by the following equation [11,12]:

$$w_s = w_{s,0}\left(\frac{T_e}{10,000\ \text{K}}\right)^b\left(\frac{N_e}{1 \times 10^{16}\ \text{cm}^{-3}}\right) \tag{35}$$

where the reference Stark width $w_{s,0}$ and the exponent b are stored in the database for each atomic line. The Doppler line half-width D_w for the Gaussian broadening is given by [6]

$$D_w = \frac{\lambda_c}{c}\sqrt{\frac{2kT_{\text{trn}}}{m}\ln 2} \tag{36}$$

where T_{trn} is the translational temperature, and m is the mass of the radiating species. The Voigt line-shape function of Eq. (32) is a function of two parameters, w_l/w_v and $\Delta\lambda/w_v$. Therefore to calculate the spectral emission and absorption coefficients broadened by the Voigt profile at any wavelength or flow condition, values of w_l/w_v from 0 to 1 and $\Delta\lambda/w_v$ from 0 to 200 are prestored at increments for w_l/w_v and $\Delta\lambda/w_v$ of 0.002 and 0.025, respectively. During the RTE calculation the line shape can be calculated using a bilinear interpolation of these stored database parameters.

Figure 1 shows the required cutoff range $\Delta\lambda/w_v$ for the half-width of the full line shape that satisfies 99.9% of the integrated emission as a function of the ratio of the Lorentzian to Voigt width for all possible N_e and T_e values. It can be seen that the cutoff range rapidly increases as the ratio of w_l/w_v increases to 2.4×10^{-2} and then remains constant. In other words, when the ratio of the Lorentzian to Voigt width is greater than 2.4×10^{-2}, the minimum cutoff limit for a single line such that it will capture 99.9% emission is 121.2.

In a thermochemical nonequilibrium flowfield the widths of different atomic lines can be vary by orders of magnitude because the change in electron number density and electron temperature in the hypersonic shock layer is large. Since this large variation in the line width can lead to different line-broadening shapes for individual atomic lines, an efficient approach to determine the proper cutoff wavelength for each atomic line is needed to accurately model emission and absorption of radiative energy in the radiative heat transport calculation. This approach is particularly important in radiative transport for the optically thick hypersonic flows considered here because transport through the line wings cannot be neglected. In the present work, the cutoff wavelength that guarantees that the emission integrated over the line shape gives 99.9% of the total line emission is stored for each line as a function of the ratio of the Lorentzian to Voigt width.

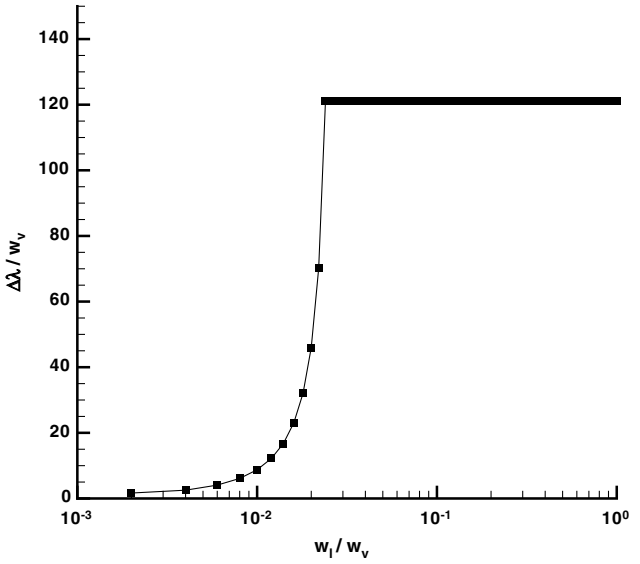

Fig. 1 Cutoff range of the Voigt line shape to satisfy 99.9% integrated line for atomic line with respect to the ratio of Lorentzian to Voigt width.

With the atomic line shape defined, the normalized emission and absorption coefficients given by Eqs. (4) and (5) are calculated for any given density, temperature, and wavelength. For the bound–free case, the normalized bound–free absorption coefficients are calculated using the bound–free cross sections, Eq. (12), and the normalized electronic state populations, N_i/N_a, which are already calculated for the bound–bound radiation. Finally, the normalized free–free absorption coefficients are obtained by Eq. (15) and computed using the density values from the flowfield solution and physical parameter data sets available from NEQAIR.

III. Basic Formulas for Radiation of Diatomic Species

Modeling of molecular radiation is more complex than for atomic species because in addition to electronic transitions, rotational and vibrational transitions must also be considered. The large number of rotational lines in a diatomic band system makes the task of determining the Einstein A coefficient for each line from the NEQAIR database complicated. In NEQAIR, the transition probabilities are calculated from a number of parameters. The expression for the Einstein A coefficient, A_{UL}, is given by [3]

$$A_{\text{UL}} = \left(\frac{64\pi^4\tilde{\nu}_{\text{UL}}^3}{3h}\right)(ea_0)^2 Re^2 q_{V_U V_L} S_{J_U J_L}/(2J_U + 1) \tag{37}$$

where

$$\tilde{\nu}_{\text{UL}} = \frac{1}{\lambda_c} = T_{eU} - T_{eL} + [G(V_U) - G(V_L)] + [F(J_U) - F(J_L)] \tag{38}$$

By using Eqs. (1) and (37), the spontaneous emission coefficient can be written as [13]

$$\varepsilon_\lambda = \frac{16\pi^3 \tilde{\nu}_{UL}^4 c}{3(2J_U+1)}(ea_0)^2 N_U g_U \mathrm{Re}^2 q_{V_U V_L} S_{J_U J_L} \phi_\lambda \tag{39}$$

where ϕ_λ is again the line-shape function and N_U is the upper state population in a given vibrational–rotational state. The normalized emission and absorption coefficients can be defined in a manner similar to the atomic cases given in Eqs. (4) and (5). Here, ε_λ^c and κ_λ^c for molecules are defined as

$$\varepsilon_\lambda^c = \frac{16\pi^3 \tilde{\nu}_{\mathrm{UL}}^4 c}{3(2J_U+1)}(ea_0)^2 g_U \mathrm{Re}^2 q_{V_U V_L} S_{J_U J_L} \tag{40}$$

$$\kappa_\lambda^c = \varepsilon_\lambda^c \frac{\lambda_c^5}{2hc^2} \tag{41}$$

To database ε_λ^c and κ_λ^c we need to determine the dependency of the quantities in Eqs. (40) and (41) on the flowfield variables. Since an electronic transition in a molecule takes place much more rapidly than a vibrational transition, in a vibronic transition, the nuclei have very nearly the same position and velocity before and after the transition [14]. A transition moment between two vibrational quantum numbers, V_U and V_L of different electronic states can therefore be approximated by [14]

$$R_{V_U V_L} = Re \int \Psi_{V_U} \Psi_{V_L} \, \mathrm{d}r \tag{42}$$

where Re is an averaged value of the electronic transition moment. The transition probability is directly proportional to $R_{V_U V_L}^2$ or $|\int \Psi_{V_U} \Psi_{V_L} \, \mathrm{d}r|^2$, where the vibrational overlap integral, $q_{V_U V_L} = |\int \Psi_{V_U} \Psi_{V_L} \, \mathrm{d}r|^2$, is called the Franck–Condon factor and does not depend on species concentrations or temperatures [14]. The line-strength factor $S_{J_U J_L}$, depends on the type of electronic transition and the spin multiplicity as well as rotational quantum number. Using standard spectroscopic relationships it can be shown that the upper state population, N_U, is given by

$$N_U = \frac{N_U^e}{(Q_{VR})_U}(2J_U+1)\exp\left[-\frac{hc}{k}\left(\frac{G(V_U)}{T_V}+\frac{F(J_U)}{T_R}\right)\right] \tag{43}$$

where N_U^e and $(Q_{VR})_U$ are the electronic upper state population and upper state total partition function, respectively. Using the above relationships, the population ratio, N_L/N_U, is given by

$$\frac{N_L}{N_U} = \frac{N_L^e}{N_U^e}\frac{(Q_{VR})_U}{(Q_{VR})_L}\left(\frac{2J_L+1}{2J_U+1}\right)\exp\left[\frac{hc}{k}\left(\frac{G(V_U)-G(V_L)}{T_V} + \frac{F(J_U)-F(J_L)}{T_R}\right)\right] \tag{44}$$

where the upper state total partition function Q_{VR} is given as [13]

$$(Q_{VR})_U = \sum_{V_U=0}^{V_U=\max}\left[\left(\sum_{J_U=0}^{J_U=\max}(2J_U+1)\exp\left(-B_{V_U}J_U(J_U+1)\right)\frac{hc}{kT_R}\right)\right) \times \exp\left(-G(V_U)\frac{hc}{kT_V}\right)\Bigg] \tag{45}$$

A. Calculation of Excited Electronic State Population for Diatomic Species

In this section, derivation of the excited electronic state populations N_U^e for diatomic species using the QSS assumption is discussed. The baseline excitation/deexcitation processes for diatomic species are modeled as

$$Z + U + W \overset{K_{Wi}}{\leftrightarrow} ZU(i) + W \tag{46}$$

$$\mathrm{e}^- + ZU^+ + \mathrm{e}^- \overset{K_{ci}^e}{\leftrightarrow} ZU(i) + \mathrm{e}^- \tag{47}$$

$$ZU(i) + W \overset{K^W(i,j)}{\leftrightarrow} ZU(j) + W \tag{48}$$

$$\mathrm{e}^- + ZU(i) \overset{K^e(i,j)}{\leftrightarrow} ZU(j) + e^- \tag{49}$$

$$ZU(i) \overset{A(i,j)}{\leftrightarrow} ZU(j) + hv \tag{50}$$

where Z and U represent atomic species, and W and e^- represent a heavy particle and an electron, respectively. Equations (46–50) represent heavy-particle- and electron-induced recombination, heavy-particle- and electron-induced excitation, and spontaneous emission, respectively [15]. The time rate of change of normalized number density, $\rho_i = N_i/N_{iE}$, is given by the difference between the incoming rates and outgoing rates [5,15]:

$$\frac{1}{N_e}\frac{\partial \rho_i}{\partial t} = \left[-\sum_{j=1}^{l_m}\left[K^e(i,j)+K^W(i,j)\frac{N_W}{N_e}+\frac{A(i,j)}{N_e}\right] + K_{ic}^e + K_{iW}\frac{N_W}{N_e}\right]\rho_i + \sum_{j=1}^{l_m}\left[K^e(i,j)+K^W(i,j)\frac{N_W}{N_e} + \frac{A(j,i)}{N_e}\frac{N_{jE}}{N_{iE}}\right]\rho_j + \left[K_{ic}^e + K_{iW}\frac{N_W}{N_e}\right] \tag{51}$$

where $K^e(i,j)$ is the electron-impact excitation rate coefficient between two electronic states of a molecule, $K^W(i,j)$ is the excitation rate coefficient by neutral impact between two electronic states, and K_{iW} and K_{ic}^e represent dissociation rate coefficients due to heavy-particle collision and electron impact, respectively. Note that the reversal of indices such as iW to Wi changes the rate coefficient from collisionally induced dissociation to a recombination mechanism. Under the QSS condition, the left-hand side is set to zero and the system of differential equations becomes a matrix equation of the form

$$M_m \bar{\rho} = \bar{C}_m + \bar{D}_m \frac{N_m}{N_Z} \tag{52}$$

where

$$N_m = \sum_{i=1}^{l_m} N_i$$

and the matrix M_m and vectors $\bar{C}_m$ and $\bar{D}_m$ are assembled by excitation and dissociation rate coefficients. The final form of the diatomic QSS relation is given as

$$\bar{\rho} = \frac{N_i}{N_{iE}} = M_m^{-1}\left(\bar{C}_m + \bar{D}_m \frac{N_m}{N_Z}\right) \tag{53}$$

The upper and lower electronic state populations, N_L^e and N_U^e, are solved by a 4×4 matrix inversion.

B. Strategy for Creating Databases of Spectral Quantities for Diatomic Emitters

In this section, databasing schemes for diatomic gas species will be introduced. First, the diatomic line-strength factors ε_λ^c given by Eq. (40) are extracted from NEQAIR and stored with line-center wavelengths. Since the vibrational term energy $G(V)$ and rotational term energy $F(J)$ are not dependent on gas concentration or temperature, these energy terms, which are needed to calculate the upper and lower state populations, will also be stored with the corresponding line-center wavelength. In this work, the assembled line-strength-factor line-center wavelength and vibrational–rotational term energy of N_2^+, NO, N_2, and O_2 are extracted from NEQAIR and stored in the database. Table 3 shows the types of electronic transitions for N_2^+, NO, N_2, and O_2 considered in NEQAIR, and Table 4 presents the first five rows of the N_2^+ first negative transition data set. The electronic state populations will be obtained from the QSS assumption and then the final forms of emission and absorption coefficients will be constructed combining the line-center data set with the electronic state populations. Similar to the atomic case, a

Table 3 Electronic transitions of diatomic species in NEQAIR

Molecule	Name	Spectral range, Å
N_2^+	1^- (first negative)	2547–25,759
N_2^+	Meinel	2749–1,645,451,798
N_2	1^+ (first positive)	4125–3,691,642
N_2	2^+ (second positive)	2602–7229
N_2	Birge–Hopfield	870–1568
N_2	Birge–Hopfield 2	827–1889
N_2	Carrol–Yoshino	845–1240
O_2	Schumann–Runge	1763–5919
NO	Beta	1681–9210
NO	Gamma	1653–5403
NO	Delta	1553–3519
NO	Epsilon	1532–4130
NO	Beta prime	1479–2913
NO	Gamma prime	1395–2229
NO	(C-A)	5700–222,006,382
NO	(D-A)	6436–47,484
NO	B'-B	4777–57,779
NO	E-C	5186–70,955
NO	F-C(3)	6087–129,110
NO	H-C	5689–110,131
NO	H'-C	5845–82,550
NO	E-D(5)	6870–38,754
NO	F-D(3)	6447–36,623
NO	H-D	7019–24,737
NO	H'-D(5)	6940–14,439
NO	IR	2986–178,078

Voigt line-shape function is assumed for each vibrational and rotational line center.

IV. Application of Radiation Databases to Reentry Flow Cases

A. Investigation of the Accuracy of Spectral Coefficients Generated Using the Database

Before considering the radiation from specific reentry flows, we discuss the accuracy of the new databasing schemes by comparing the emission and absorption coefficients with those obtained from NEQAIR. Figures 2 and 3 show comparisons between the database and NEQAIR of the emission and absorption coefficients of atomic O for the wavelength range from 500 to 2000 Å with a wavelength increment of 0.003 Å and from 2000 to 7000 Å with 0.005 Å steps. For this comparison the database and NEQAIR use the Voigt line-shape function. The density and temperature conditions were obtained from the flowfield solution of the Stardust vehicle with a speed of 12 km/s at 81 km altitude, calculated using the direct simulation Monte Carlo (DSMC) method. The conditions represent the location in the flow where high radiation occurs due to the high electron temperature. The error in the emission and absorption coefficients is defined as

$$\text{error}\,(\%) = \left(\frac{|X_{i,\text{data}} - X_{i,\text{NEQ}}|}{|X_{i,\text{NEQ}}|}\right) \times 100 \tag{54}$$

where $X_{i,\text{data}}$ and $X_{i,\text{NEQ}}$ are the emission or absorption coefficients from the database and NEQAIR at the ith wavelength data point, respectively. In this comparison, most of the errors between the database and NEQAIR are observed to be smaller than 1%, except for the continuum radiation below 800 Å and the bound–bound transitions at 5331 and 6158 Å. The error at 5331 Å is due to the overlap of the line-shape functions in the wings of each of the three atomic oxygen transitions, all closely located at 5330.46, 5331.07, and 5332.14 Å. The error observed at 6158 Å is due to a similar problem. The continuum spectral coefficients for both bound–free and free–free transitions are linearly interpolated using the precalculated values stored in increments of 1 Å. As discussed in the previous section, bound–free transitions occur in spectral regions with sharp wavelength start and stop intervals. Because there is a delta-function-like cutoff, the linear interpolation error can be larger, due to large gradients in the emission and absorption lines with respect to wavelength. Figures 4 and 5 show the comparisons of the emission and absorption coefficients for atomic N between the database and NEQAIR for the range from 500 to 7000 Å. Again, the error in the emission and absorption coefficients of atomic N are below 1.0%.

Now we compare the bound–bound line strengths and continuum spectral coefficients of atomic species generated from the database with those from NEQAIR for the entire range of N_e and T_e conditions. The bound–bound emission line strengths and continuum spectral coefficients at three interior points between two successive data points of N_e and T_e were generated and compared with NEQAIR. The maximum error in the bound–bound emission line strength of atomic O and N was found to be within 0.12% for the entire range of N_e and T_e conditions. Since the emission line strength is proportional to the upper state electronic population, the comparison shows that the electronic state populations of atomic O and N are well predicted by the database and interpolation schemes. For the absorption bound–bound line strength, it was observed that below 10,000 K there are some absorption line-strength errors greater than 3%, but this was the largest discrepancy observed. Since the absorption line strength is proportional to the difference of the lower and upper electronic state populations, the error in the difference may be larger than the error in the upper electronic state population. However, there are only 1702 absorption line strengths that have errors of over 3% out of a total of 15,904,000 cases (200 for N_e points × 280 for T_e points × 284 for lines for N and O). Since the ratio of absorption line strengths with error greater than 3% to the maximum absorption line strength is within 10^{-4}, this larger error of 3% does not affect the radiation calculation.

The average error in the continuum emission and absorption coefficients was also investigated. Since the absorption and emission coefficients of the bound–free transition are related to the electronic state population as given by Eqs. (12) and (13), respectively, the accuracy of the bound–free spectral coefficients depends on the error of the electronic state populations. As discussed earlier in the bound–bound line-strength comparisons, the electronic state populations calculated from the database agree well those from NEQAIR, and thus the bound–free spectral coefficients obtained from the database are expected to be in a good agreement with those of NEQAIR. The free–free absorption and emission coefficients are calculated directly in terms of number density and electron temperature, as given by Eqs. (15) and (16), respectively. Therefore the only difference between the continuum spectral coefficients obtained from the database and NEQAIR can occur from the bound–free transitions. The error in the continuum spectral coefficient was investigated for a range of 500 to 10,500 Å with a 0.2 Å wavelength increment. The same number of N_e and T_e conditions used in the bound–bound line-strength comparisons (200 for N_e points × 280 for T_e points) were considered, again, to cover all possible flow conditions. Finally, the

Table 4 Data set example for N_2^+ first negative transition

Wavelength, Å	ε_λ^c, W/sr	$-\frac{hc}{k}G(V_U)$, K	$\frac{hc}{k}F(J_U)$, K	$\frac{hc}{k}(G(V_L) - G(V_U))$, K	$\frac{hc}{k}(F(J_L) - F(J_U))$, K
2547.335	1.149×10^{-15}	-3.486×10^4	-1.265×10^2	1.968×10^4	16.318
2547.340	9.848×10^{-16}	-3.486×10^4	-9.488×10^1	1.968×10^4	16.210
2547.353	1.149×10^{-15}	-3.486×10^4	-1.265×10^2	1.968×10^4	15.915
2547.355	9.847×10^{-16}	-3.486×10^4	-9.487×10^1	1.968×10^4	15.865
2547.364	1.313×10^{-15}	-3.486×10^4	-1.626×10^2	1.968×10^4	15.679

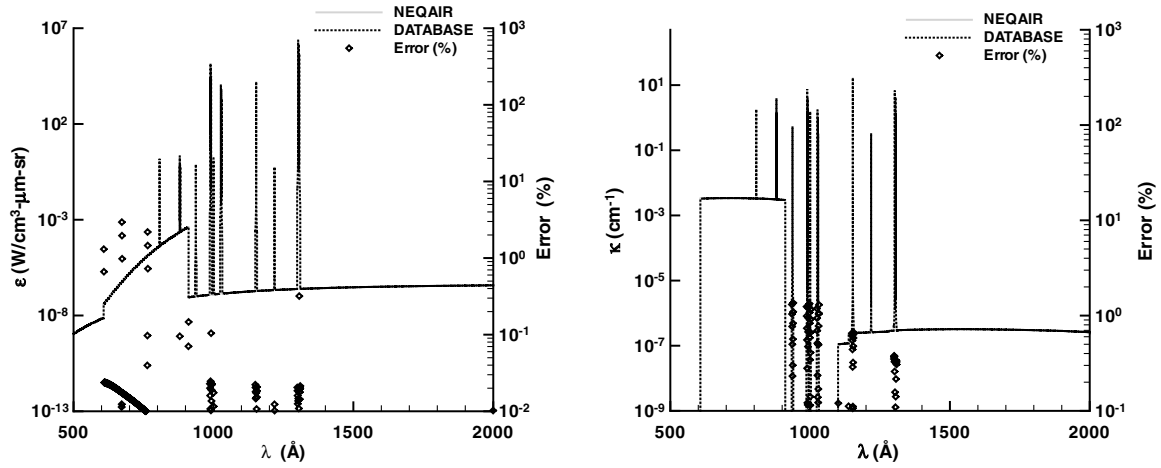

Fig. 2 Comparison of emission and absorption coefficients of atomic O from 500 to 2000 Å between the database and NEQAIR for $N_a = 1.1513 \times 10^{15}$ cm^{-3}, $N_+ = 3.8214 \times 10^{12}$ cm^{-3}, $N_e = 1.2667 \times 10^{14}$ cm^{-3}, $T_{\text{trn}} = 24,187$ K, and $T_e = 17,485$ K.

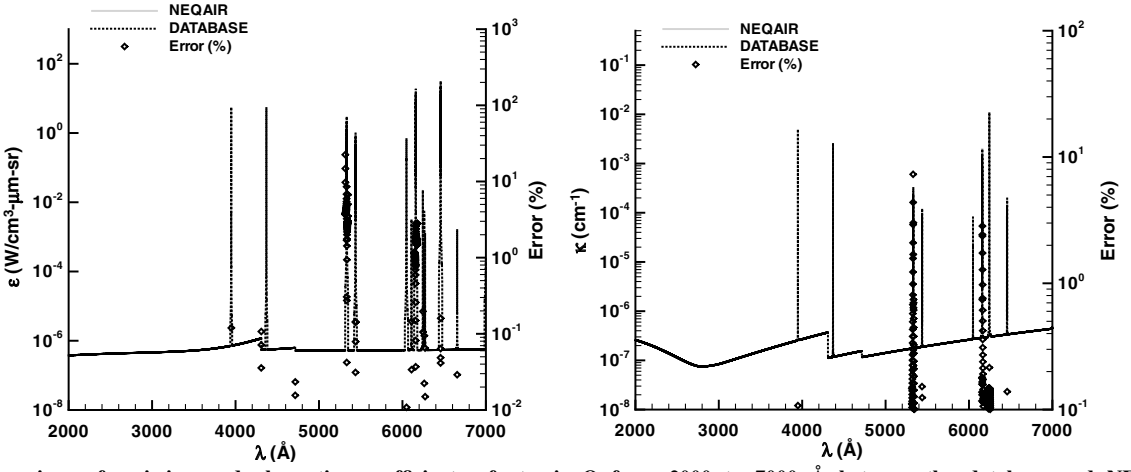

Fig. 3 Comparison of emission and absorption coefficients of atomic O from 2000 to 7000 Å between the database and NEQAIR for $N_a = 1.1513 \times 10^{15}$ cm^{-3}, $N_+ = 3.8214 \times 10^{12}$ cm^{-3}, $N_e = 1.2667 \times 10^{14}$ cm^{-3}, $T_{\text{trn}} = 24,187$ K, and $T_e = 17,485$ K.

average error in the continuum emission and absorption coefficients was found to be less than 0.05 and 0.03%, respectively.

With respect to radiation from molecular species, Figs. 6–9 show the emission and absorption coefficients from NEQAIR and the absolute difference of coefficients between the database and NEQAIR for the N_2^+, NO, N_2 and O_2 molecular systems, respectively. There are small differences between the databasing scheme and NEQAIR mainly due to the difference in the implementation of the Voigt line shape. NEQAIR uses an approximate approach to define the Voigt line shape for each rotational line. In our databasing scheme we use a more accurate procedure to apply the Voigt line shape with no additional computational cost. A summary of the differences in the

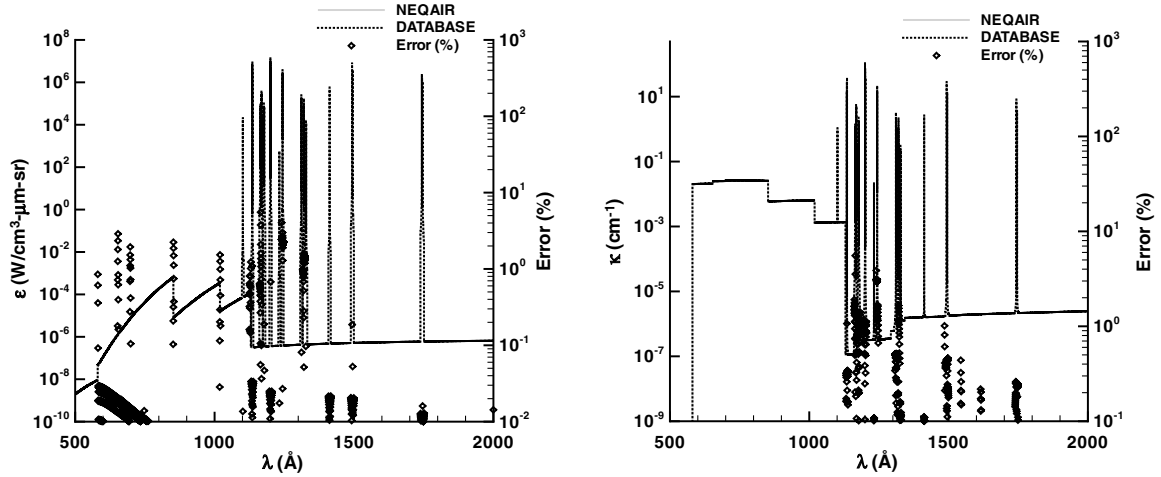

Fig. 4 Comparison of emission and absorption coefficients of atomic N from 500 to 2000 Å between the database and NEQAIR for $N_a = 3.1609 \times 10^{15}$ cm^{-3}, $N_+ = 5.5472 \times 10^{12}$ cm^{-3}, $N_e = 1.2667 \times 10^{14}$ cm^{-3}, $T_{\text{trn}} = 24,187$ K, and $T_e = 17,485$ K.

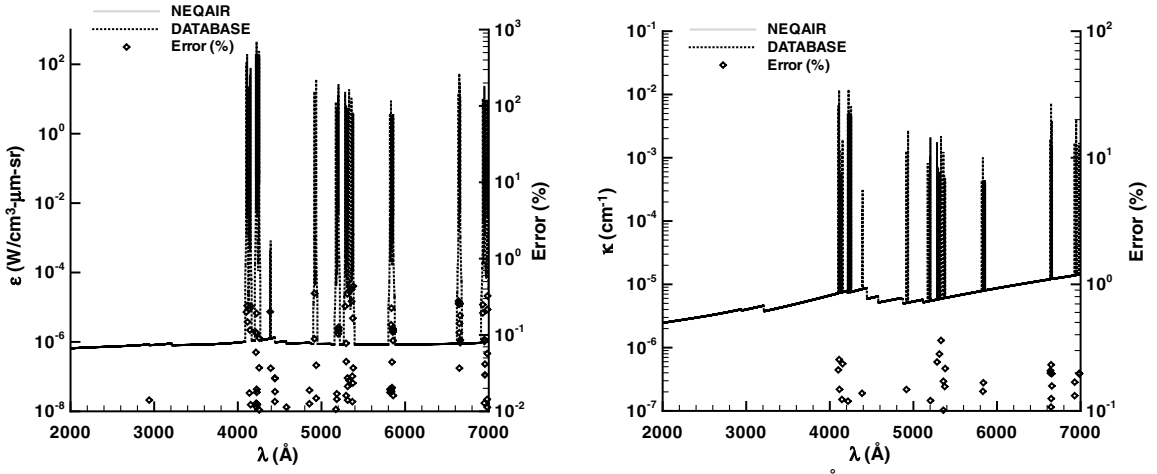

Fig. 5 Comparison of emission and absorption coefficients of atomic N from 2000 to 7000 Å between the database and NEQAIR for $N_a = 3.1609 \times 10^{15}$ cm^{-3}, $N_+ = 5.5472 \times 10^{12}$ cm^{-3}, $N_e = 1.2667 \times 10^{14}$ cm^{-3}, $T_{\text{trn}} = 24,187$ K, and $T_e = 17,485$ K.

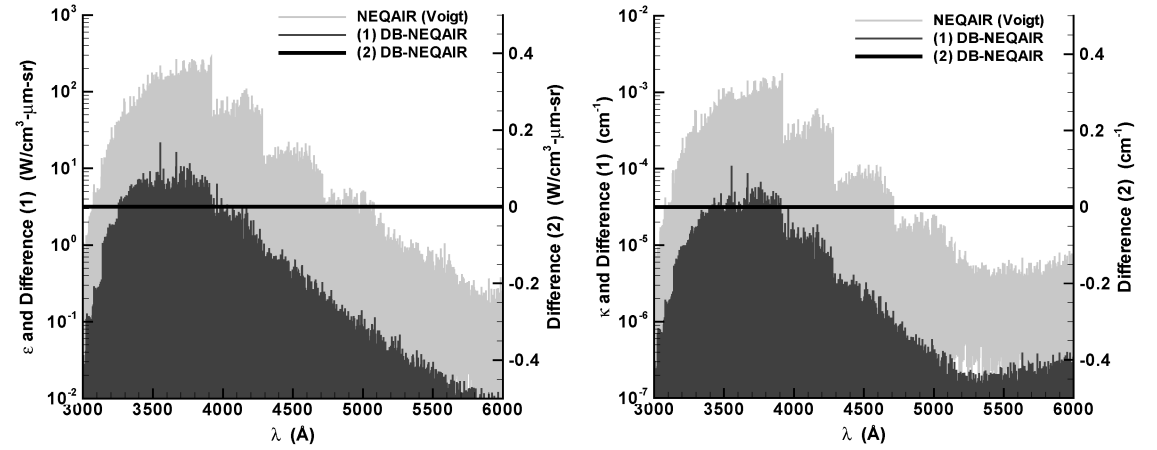

Fig. 6 Comparison of emission and absorption coefficients of N_2^+ from 3,000 to 6,000 Å between the database and NEQAIR for $N_{N_2^+} = 6.4529 \times 10^{13}$ cm^{-3}, $N_N = 3.9464 \times 10^{15}$ cm^{-3}, $N_e = 1.1607 \times 10^{14}$ cm^{-3}, $T_{\text{trn}} = 34,469$ K, and $T_e = 16,511$ K.

procedures is as follows. In NEQAIR, the Voigt width is assumed to be constant for a given vibrational band, whereas in the present databasing scheme, the Voigt line width is calculated at the line-center wavelength of each vibrational–rotational line. NEQAIR prepares a template for the Voigt line shape for a single rotational line in the vibrational–rotational transition. The same template is then copied to all the lines in that particular vibrational band. In the databasing scheme, different line shapes are used for each vibrational–rotational line center. The value of line-shape function is not calculated exactly at the desired spectral point in NEQAIR. Rather, it is assumed that some of the spectral points coincide with the line-center wavelength. The line-shape function is thus approximated by the value at a wavelength fixed a distance away from the line-center wavelength. In the databasing scheme, the line-shape function is calculated at the exact wavelength position. In NEQAIR, whether the contribution from a line is important or not is determined by a cutoff limit based on

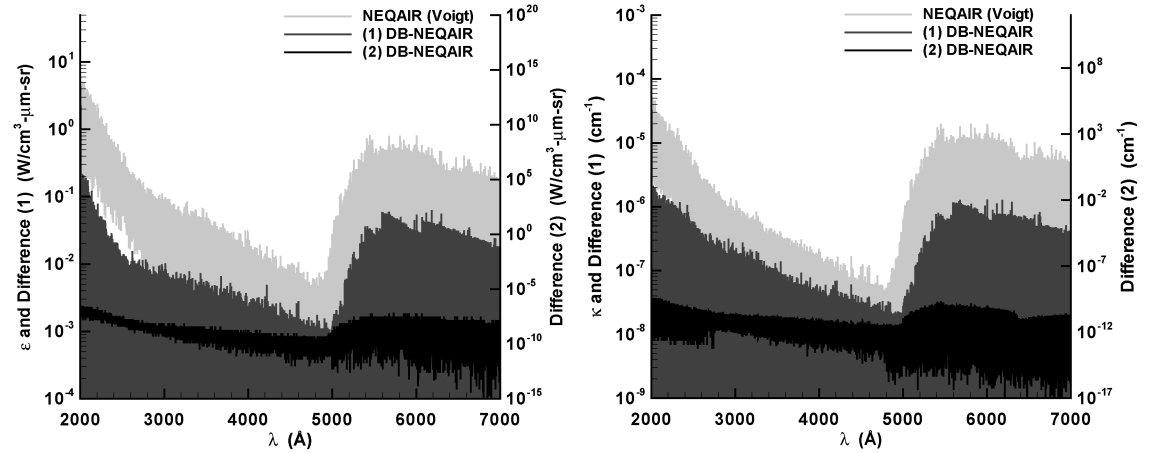

Fig. 7 Comparison of emission and absorption coefficients of NO from 2000 to 7000 Å between the database and NEQAIR for $N_{\text{NO}} = 2.5624 \times 10^{13}$ cm^{-3}, $N_N = 3.9464 \times 10^{15}$ cm^{-3}, $N_O = 1.2829 \times 10^{15}$ cm^{-3}, $N_e = 1.1607 \times 10^{14}$ cm^{-3}, $T_{\text{trn}} = 34,469$ K, and $T_e = 16,511$ K.

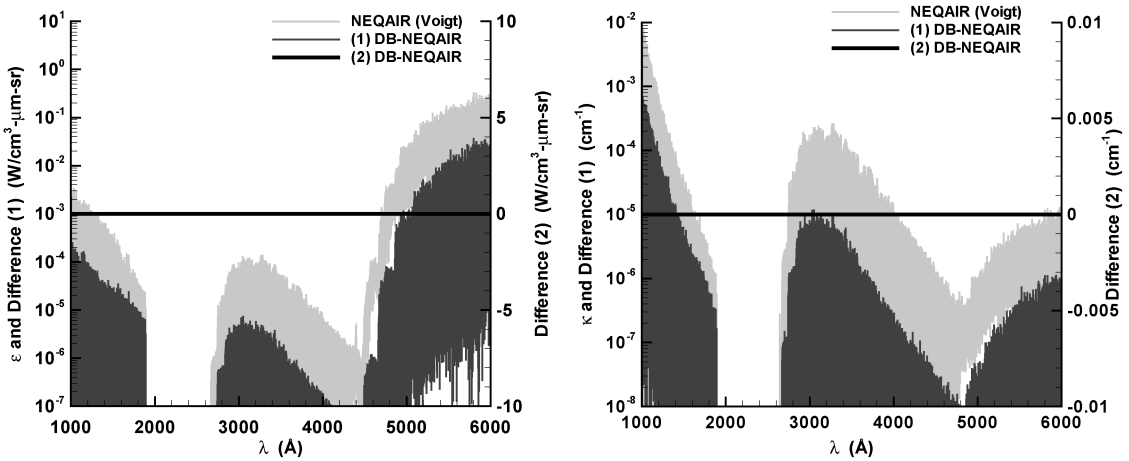

Fig. 8 Comparison of emission and absorption coefficients of N_2 from 1000 to 6,000 Å between the database and NEQAIR for $N_{N_2} = 2.5624 \times 10^{13}$ cm^{-3}, $N_N = 3.9464 \times 10^{15}$ cm^{-3}, $N_e = 1.1607 \times 10^{14}$ cm^{-3}, $T_{trn} = 34,469$ K, and $T_e = 16,511$ K.

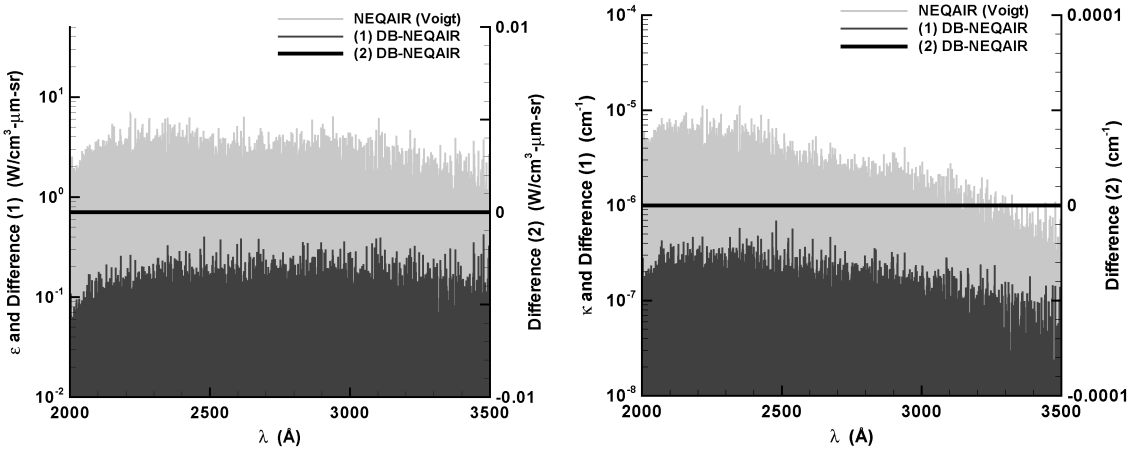

Fig. 9 Comparison of emission and absorption coefficients of O_2 from 2000 to 3,500 Å between the database and NEQAIR for $N_{O_2} = 6.8349 \times 10^{12}$ cm^{-3}, $N_O = 1.2829 \times 10^{15}$ cm^{-3}, $N_e = 1.1607 \times 10^{14}$ cm^{-3}, $T_{trn} = 34,469$ K, and $T_e = 16,511$ K.

the emission line strength, whereas in the database, we specify two separate cutoff limits on emission and absorption line strength. The absorption limit is specified as a fixed value and the emission cutoff limit is related to the absorption cutoff limit according to the following relation:

$$\varepsilon_{\min} = \kappa_{\min} \frac{2hc^2}{\lambda_c^5[\exp(hc/\lambda_c kT) - 1]} \tag{55}$$

The emission cutoff limit changes each line differently. In the database scheme we are interested in retaining some of the lines which are not important from the emission point of view but are important from the absorption point of view and vice versa.

To verify the accuracy of the new databasing schemes for diatomic species, the emission and absorption coefficients from the database and NEQAIR are compared using the same Voigt line distribution method for both the database and NEQAIR. The accuracy of the databasing scheme is temporarily degraded in order to compare as closely as possible with the NEQAIR approach. In this comparison the four methods for the distribution of Voigt line-shape function are applied to the database and NEQAIR. Voigt widths are determined at the vibrational band center. The line-center wavelength in Eq. (33) is defined for each different vibrational–rotational transition. Emission and absorption coefficients at a given wavelength are approximated using the nearest spectral data point in NEQAIR. The emission and absorption coefficients are also directly calculated in the database using the same approach. The emission cutoff limit is used as a single value, given by NEQAIR, for the entire spectral region. Figures 6–9 also show the absolute difference of spectral coefficients between the database and NEQAIR calculated under the same Voigt line distribution method. It can be seen that there is excellent agreement between the emission and absorption coefficients predicted by the temporarily degraded database and NEQAIR.

B. Investigation of Databasing Scheme Efficiencies

The objective of this work is to create a database that can be used in calculating the spectral coefficients efficiently. This is essential for the coupled study of radiation heat transfer in hypersonic nonequilibrium flowfields. These databasing schemes provide an efficient way for calculating the spectral coefficients for full as well as narrow wavelength ranges. For molecular band calculation, all the rotation–vibration lines that contribute to the spectral coefficients at each given wavelength, are stored in the database. The spectral coefficients for a given narrowband can be efficiently generated using this information. Note that the basic database, example shown in Table 4, is read only once and the actual computational time of the database is much less than that of NEQAIR because it is not needed to repeat many arithmetical operations to calculate the basic radiation parameters. The CPU times of the dual 2.4 GHz AMD Opteron processors shown in Tables 5 and 6 clearly demonstrate that by using our new database scheme spectral coefficients can be generated more efficiently both for a large wavelength range and for small narrowbands than by the present procedure in NEQAIR. In this CPU time study, the wavelength increment is 0.05 Å, and 20 gas cells were considered from the stagnation line flow condition of Stardust at the 68.9 km altitude calculated by DSMC. In these gas cells, the electron

Table 5 Comparison of computation time for narrow spectral region from 500 to 2000 Å

Species	NEQAIR	Database
Atomic species	5.33 s	0.36 s
Diatomic species	12.15 s	3.86 s
All species	17.27 s	3.55 s

Table 6 Comparison of computation time for wide spectral region from 500 to 10,000 Å

Species	NEQAIR	Database
Atomic Species	48.65 s	2.13 s
Diatomic Species	230.33 s	75.41 s
All Species	279.90 s	79.05 s

temperature varies from 5252 to 19,846 K. Atomic N and O bound–bound, bound–free, and free–free transitions and six molecular bands (first negative for N_2^+, first and second positive for N_2 and β, and γ for NO and Schumann–Runge for O_2) were considered in this example. Because we use an efficient interpolation scheme for generating atomic spectral coefficients, there is large savings of computational time for the atomic calculations. The data interpolation scheme provides an efficient and accurate means for generating spectral coefficients for atomic bound–bound, bound–free, and free–free transitions.

The efficiency of applying a variable cutoff range in the atomic radiation calculation was also examined. Atomic O and N bound–bound radiation was considered, and 40 gas layers were used from the stagnation line flow of a Stardust flowfield at the 68.9 km altitude simulated by DSMC method. The wavelength range from 100 to 20,000 Å was assumed to capture emission far from the line center for all the lines and the spectral resolution was 0.0025 Å. The error in the total emission energy,

$$E_{\text{emis}} = 4\pi \int_{\lambda} \varepsilon \, \mathrm{d}\lambda$$

between the integrated emission obtained using a variable and a fixed cutoff range compared with the summation of the line strengths of all atomic lines is shown in Fig. 10 for each cell along the stagnation streamline. A value of 121.2 was chosen as the fixed value for all atomic bound–bound transitions because, as shown earlier, it captures 99.9% of the total emission energy for all ratios of Lorentzian to Voigt widths. From the figure it can be seen that the variable cutoff range satisfies 99.9% total emission energy. The variable cutoff range scheme leads to a reduction of computational time because the unnecessarily large cutoff range is not applied to all atomic lines. The CPU time for the calculation using the variable range is 16.4 s, whereas using the fixed cutoff range it was found to be 20.72 s. Most of the atomic lines in the spectral region below 2000 Å need to use a value of 121.2 as the cutoff range to satisfy the 99.9% total emission energy criteria, under the high electron number density and electron temperature gas conditions. Therefore, only a reduction of about 20% in computational time was achieved. However, when iterative calculations are used, such as in the photon Monte Carlo RTE, and in highly optically thick conditions [16,17], this reduction of the computational time without loss of accuracy will be important.

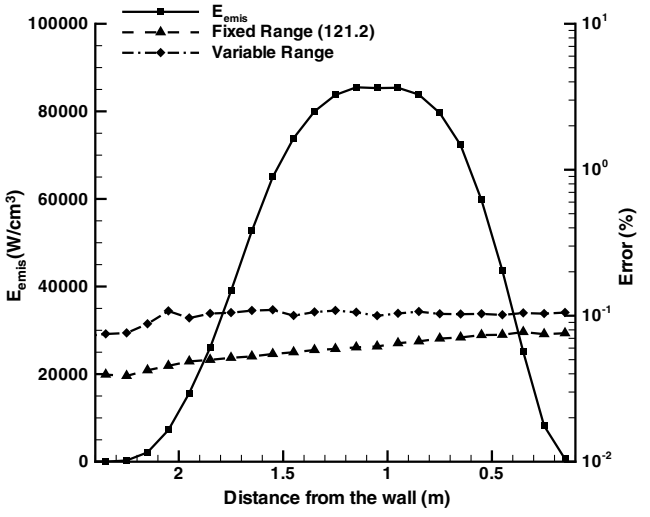

Fig. 10 Comparison of total emission energy error using fixed and variable cutoff ranges for atomic bound–bound radiation along the stagnation line of Stardust at 68.9 km altitude.

Table 7 Free stream conditions of Stardust reentry flow

	CFD	DSMC 1	DSMC 2
Altitude, km	61.76	68.9	81.0
Velocity, m/s	10.871	11,902	12,800
Temperature, K	234.95	224.0	217.6
Number density, m^{-3}	4.407×10^{21}	1.603×10^{21}	2.639×10^{20}

C. Application of Databasing Schemes to Radiation Calculations

In the previous section, we have shown that the database procedure calculates emission and absorption coefficients accurately for a single flowfield condition. As the final verification of our databasing scheme, we have used it to demonstrate the calculation for radiative heat generation rate along the stagnation line and a flowfield condition close to the shoulder line of the Stardust vehicle. For nonequilibrium gas conditions, calculations of radiative heat generation require data for both the emission and absorption coefficients. Thus, the objective of this work is to verify the reliability of the emission and absorption coefficients through the radiative heat generation computation for all possible flow conditions. In this work, flowfield solutions for three free stream conditions were used to provide species concentrations and temperatures in each cell. The radiation computation was performed using the tangent-slab approximation and radiative results obtained from the new databasing schemes were compared with those of NEQAIR. Because of the fact that diatomic species contribute much less to the radiative heat flux compared with atomic emitters, it is not necessary to use a fine wavelength resolution for the entire wavelength range. Hence, a variable wavelength increment in this calculation was used as follows: $\Delta\lambda = 0.005$ Å for 500 to 5000 Å and $\Delta\lambda = 0.01$ Å for 5000 to 14,000 Å.

Radiative transfer calculations were performed along two lines: the stagnation streamline and one of the lines normal to the vehicle shoulder body. The flowfield solutions are obtained from the data-parallel line relaxation (DPLR) computational fluid dynamics (CFD) code [18] and direct simulation Monte Carlo (DSMC) method [19]. The free stream conditions of each flow solver are listed in Table 7.

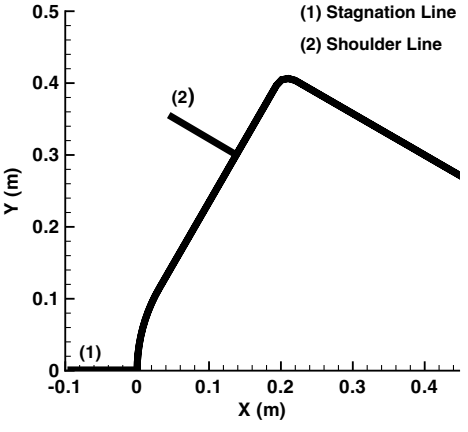

Fig. 11 Geometry of the Stardust vehicle.

These flow solvers include chemical reaction processes of 11 species such as N, O, N^+, O^+, N_2, O_2, NO, N_2^+, O_2^+, NO^+, and e^-. Figure 11 shows the locations of the stagnation stream line and shoulder line for the Stardust vehicle. For the two locations, the radiative heat generation per unit volume was calculated using the database and compared with the results of NEQAIR. The spatial distribution of number densities of the six radiating species such as N, O, N_2^+, NO, N_2, O_2, and e^- and the temperature along the stagnation line and the shoulder line of DPLR flowfield are shown in Figs. 12 and 13, respectively. It can be seen that atomic species such as N and O are

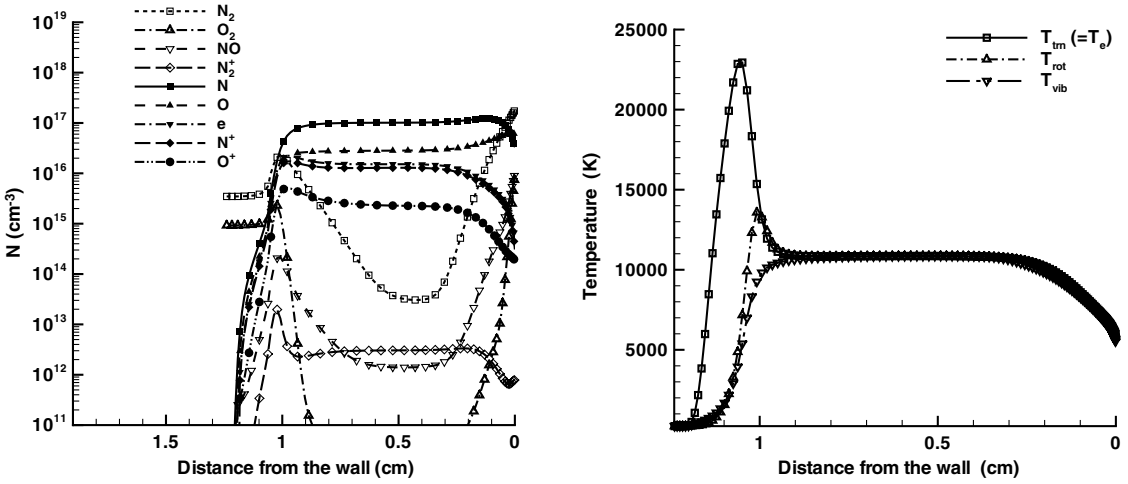

Fig. 12 Number density (left) and temperature (right) profile along the stagnation streamline of DPLR flowfield.

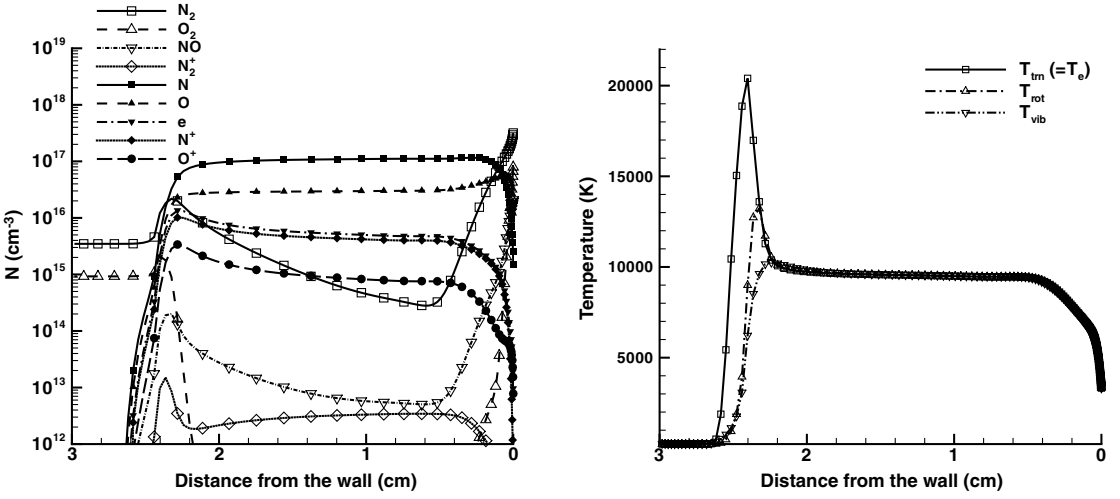

Fig. 13 Number density (left) and temperature (right) profile along the shoulder line of DPLR flowfield.

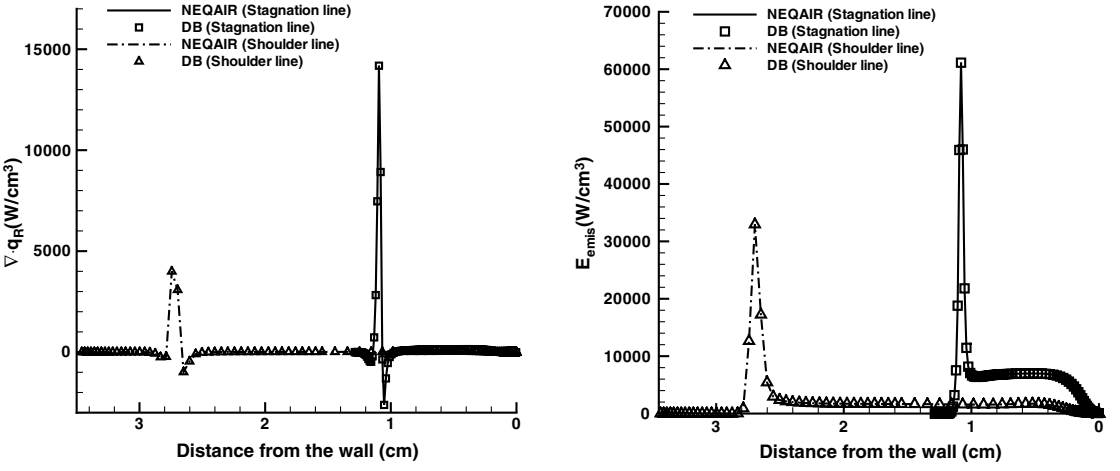

Fig. 14 Comparison of $\nabla \cdot q_R$ (left) and total emission (right) of 6 radiating species between the database and NEQAIR along the stagnation line and shoulder line of Stardust DPLR flowfield.

dominant in the shock layer, due to the strong dissociation of the molecular species. The figure also shows that the electron number density is high in the shock layer, due to ionization processes in the shock.

Figure 14 shows comparison of the total emission and radiative heat generation per unit volume from the aforementioned six radiating species calculated using the database and NEQAIR. The horizontal axis in Fig. 14 indicates the distance from the vehicle wall. In these calculations, all three types of transitions for the two atomic species and 26 electronic band systems of the four diatomic species were considered. Since electron temperature is not calculated directly in the DPLR CFD flow solver, it is assumed to be equal to

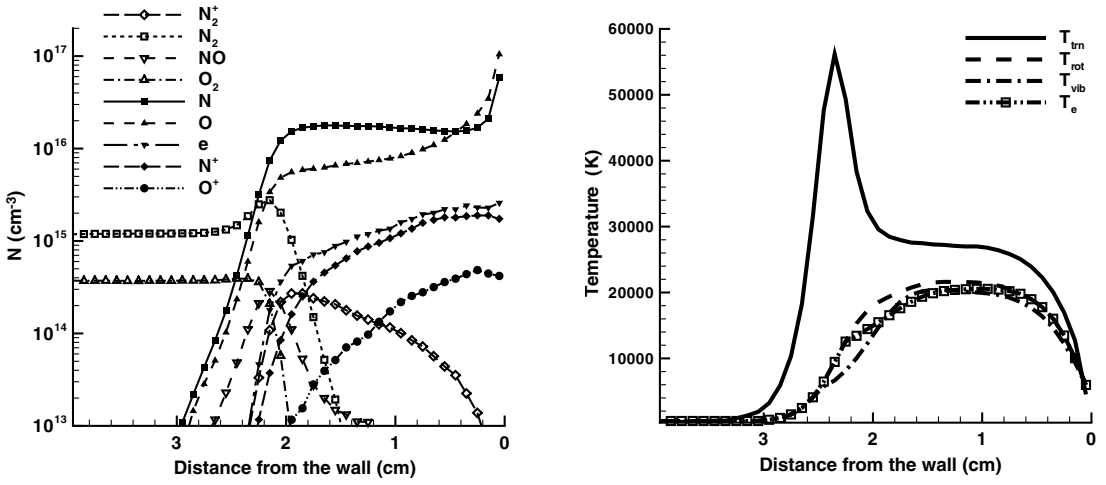

Fig. 15 Number density (left) and temperature (right) profile along the stagnation streamline of DSMC flowfield at 68.9 km altitude.

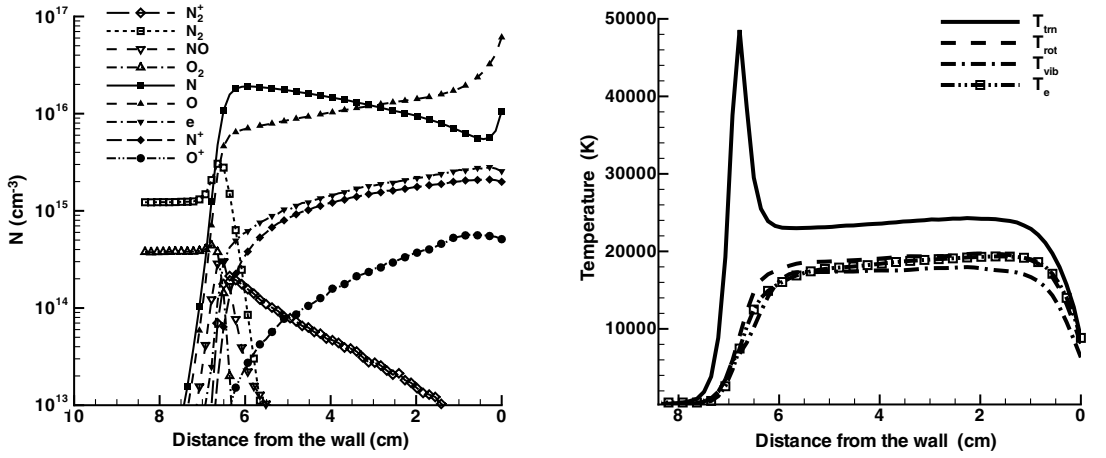

Fig. 16 Number density (left) and temperature (right) profile along the shoulder line of DSMC flowfield at 68.9 km altitude.

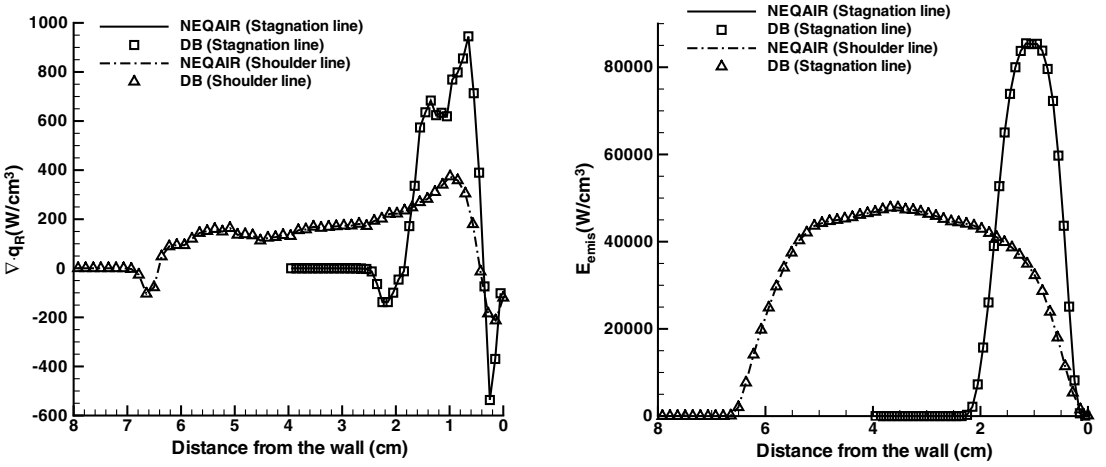

Fig. 17 Comparison of $\nabla \cdot q_R$ (left) and total emission (right) of 6 radiating species between the database and NEQAIR along the stagnation line and shoulder line of Stardust DSMC flowfield at 68.9 km altitude.

translational temperature for radiation calculation using the database and NEQAIR. To confirm the accuracy of the emission coefficients from the database, total emission along the two lines was compared with NEQAIR results. Because of the fact that radiation from atomic species is dependent on electron temperature, location of the maximum peak heat generation coincides with that of the maximum electron temperature. Good agreement of radiative heat generation and total emission between the new database and NEQAIR is obtained with errors below 0.5% in the peak heating region. Figures 15–19 show number densities and temperature profiles along the stagnation line and shoulder line obtained from the DSMC flowfield at 68.9 and 81 km altitudes, respectively. Figures 17–20

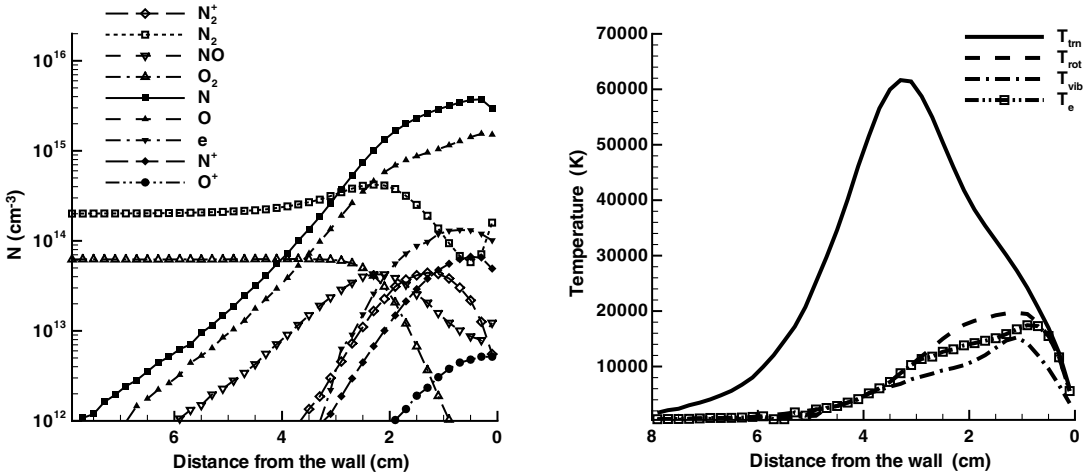

Fig. 18 Number density (left) and temperature (right) profile along the stagnation streamline of DSMC flowfield at 81 km altitude.

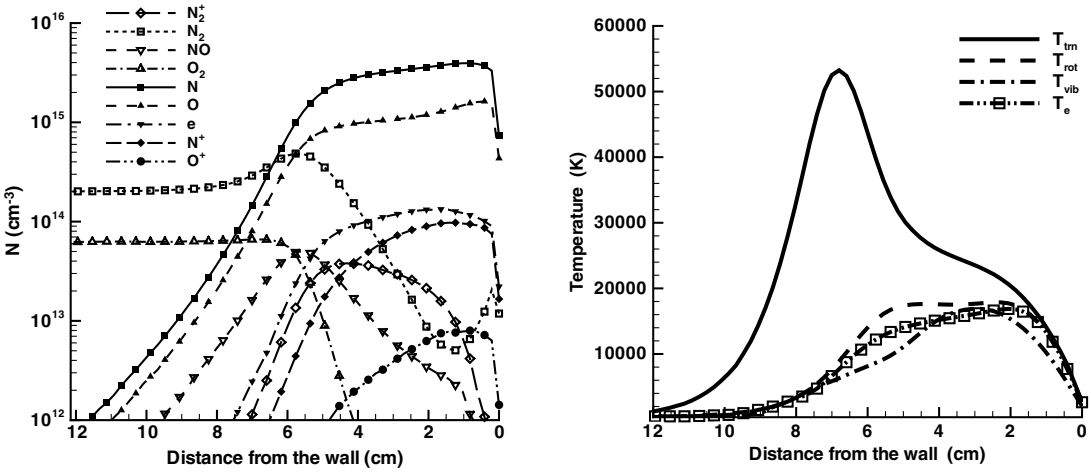

Fig. 19 Number density (left) and temperature (right) profile along the shoulder line of DSMC flowfield at 81 km altitude.

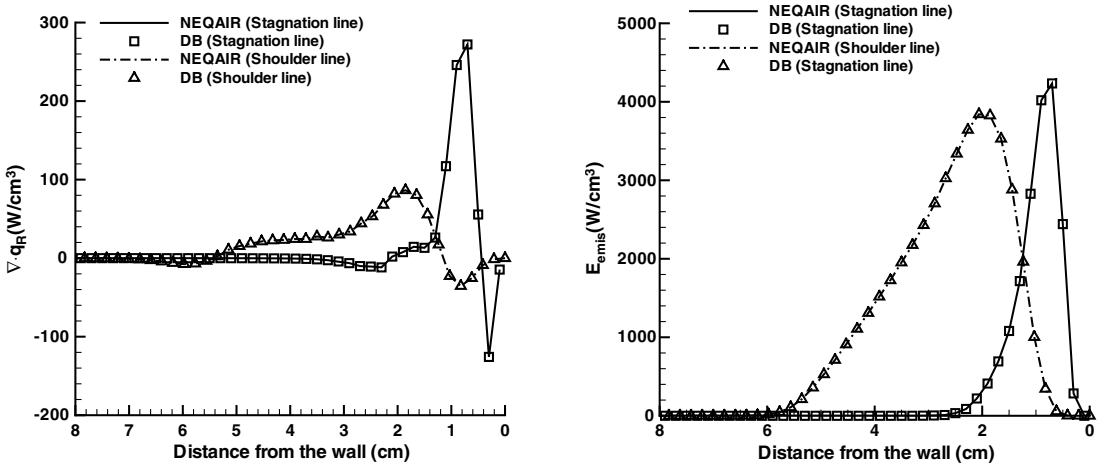

Fig. 20 Comparison of $\nabla \cdot q_R$ (left) and total emission (right) of 6 radiating species between the database and NEQAIR along the stagnation line and shoulder line of Stardust DSMC flowfield at 81 km altitude.

show that the new database and NEQAIR predict the same amount and spatial dependency for radiative heat generation and total emission along the stagnation line and shoulder line of the Stardust blunt body at 68.9 and 81 km altitudes, respectively. In the DSMC method, the electron temperature can be directly calculated and is predicted to be lower than the total averaged translational temperature in the shock layer for both 68.9 and 81 km altitudes. From the figures, it can be seen that the database and NEQAIR predict that there is significant heat generation and total emission created in the high electron number density and electron temperature region. This result is reasonable because radiation from atomic species is strongly dependent on electron number density and temperature. For the stagnation streamline and shoulder line, it is found that the radiative heat generation calculated using the spectral data from the database is in good agreement with NEQAIR with an error below 1% in the high radiative heating region.

V. Conclusions

New databasing schemes have been developed for advanced radiation calculations of hypersonic nonequilibrium reentry flows. Because of the nonequilibrium flow conditions, the quasi-steady-state assumption was used for generating the electronic state populations of atomic and diatomic gas species. A Voigt line-broadening function was used to describe the line shape of bound–bound spectral lines. The emission and absorption coefficients for any given flow condition and wavelength range were accurately and efficiently calculated using the database and its associated interpolation schemes. Comparisons of the emission and absorption coefficients for atomic O and N between the database and NEQAIR were performed to validate the accuracy of the databases and good agreement within 1% error was observed. For diatomic species N_2^+, NO, N_2, and O_2, there are some differences of results between the database and NEQAIR. This is because the broadening method as implemented in NEQAIR is different from that used in the database. It is also found that there is excellent agreement for spectral coefficients when the same broadening method was applied to both the database and NEQAIR. Radiative heat generation for the Stardust reentry for two different flowfields computed using CFD and DSMC methods, was calculated using the database. The radiative heat production from the databasing schemes predicts the same magnitude and spatial distribution as NEQAIR more efficiently. The improved computational method will have a significant impact for coupled radiation/gas-dynamic calculations.

Acknowledgment

The research performed at the Pennsylvania State University was supported through the NASA grant no. NNX07AC47A.

References

[1] Ozawa, T., "Improved Chemistry Models for DSMC Simulations of Ionized Rarefied Hypersonic Flows," Ph.D. Thesis, Department of Aerospace Engineering, Pennsylvania State Univ., University Park, PA, 2007.

[2] Hartung, L. C., "Development of a Nonequilibrium Radiative Heating Prediction Method for Coupled Flowfield Solutions," *Journal of Thermophysics and Heat Transfer*, Vol. 6, No. 4, 1992, pp. 618–625. doi:10.2514/3.11542

[3] Whiting, E. E., Park, C., Liu, Y., Arnold, J. O., and Paterson, J. A., "NEQAIR 96 User Manual," NASA Ames Research Center, Moffett Field, CA, 1996.

[4] Johnston, C. O., "Nonequilibrium Shock-Layer Radiative Heating for Earth and Titan Entry," Ph.D. Thesis, Department of Aerospace Engineering, Virginia Polytechnic Inst. and State Univ., Blacksburg, VA, 2006.

[5] Park, C., *Nonequilibrium Hypersonic Aerothermodynamics*, Wiley, New York, 1990.

[6] Modest, M. F., *Radiative Heat Transfer*, 2nd ed., Academic Press, New York, 2003.

[7] Peach, G., "Continuous Absorption Coefficient for Non-Hydrogenic Atoms," *Memoirs of the Royal Astronomical Society*, Vol. 73, 1970, pp. 1–123.

[8] Zel'dovich, Y. B., and Raizer, Y. P., *Physics of Shock Waves and High-Temperature Hydrodynamic Phenomena*, Academic Press, London, 1966.

[9] Whiting, E. E., "An Empirical Approximation to the Voigt Profile," *Journal of Quantitative Spectroscopy and Radiative Transfer*, Vol. 8, No. 6, 1968, pp. 1379–1384. doi:10.1016/0022-4073(68)90081-2

[10] Olivero, J. J., and Longbothum, R. L., "Empirical Fits to the Voigt Line Width: A Brief Review," *Journal of Quantitative Spectroscopy and Radiative Transfer*, Vol. 17, No. 2, 1977, pp. 233–236. doi:10.1016/0022-4073(77)90161-3

[11] Griem, H. R., *Spectral Line-broadening by Plasmas*, Academic Press, New York, 1974.

[12] Wilson, K. H., and Nicolet, W. E., "Spectral Absorption Coefficients of Carbon, Nitrogen and Oxygen Atoms," *Journal of Quantitative Spectroscopy and Radiative Transfer*, Vol. 7, No. 6, 1967, pp. 891–941. doi:10.1016/0022-4073(67)90005-2

[13] Arnold, J. O., Whiting, E. E., and Lyle, G. C., "Line by Line Calculation of Spectra from Diatomic Molecules and Atoms assuming A Voigt Line Profile," *Journal of Quantitative Spectroscopy and Radiative Transfer*, Vol. 9, No. 6, 1969, pp. 775–798. doi:10.1016/0022-4073(69)90075-2

[14] Herzberg, G., *Molecular Spectra and Molecular Structure 1. Spectra of Diatomic Molecules*, D. Van Nostrand, New York, 1950.

[15] Levin, D. A., Braunstein, M., Candler, G. V., Collins, R. J., and Smith, G. P., "Examination of Theory for Bow Shock Ultraviolet Rocket Experiments-II," *Journal of Thermophysics and Heat Transfer*, Vol. 8, No. 3, 1994, pp. 453–459. doi:10.2514/3.564

[16] Ozawa, T., Wang, A., Modest, M. F., and Levin, D. A., "Development of a Coupled DSMC: Particle Photon Monte Carlo Method for Simulating Atomic Radiation in Hypersonic Reentry Flows," AIAA Paper 2008-3916, June 2008.

[17] Sohn, I., Ozawa, T., Levin, D. A., and Modest, M. F., "DSMC Hypersonic Reentry Flow Simulations with Photon Monte Carlo Radiation," AIAA Paper 2009-1566, Jan. 2009.

[18] Wright, M., Candler, G. V., and Bose, D., "Data-Parallel Line Relaxation Method for the Navier-Stokes Equations," *AIAA Journal*, Vol. 36, No. 9, 1998, pp. 1603–1609. doi:10.2514/2.586

[19] Ozawa, T., Zhong, J., and Levin, D. A., "Development of Kinetic-Based Energy Exchange Models for Noncontinuum, Ionized Hypersonic Flows," *Physics of Fluids*, Vol. 20, 2008, Paper 046102. doi:10.1063/1.2907198